Structural Eng./Earthquake Eng., JSCE, Vol. 18, No. 2, 111s—127s, 2001 October
(J. Struct. Mech. Earthquake Eng., JSCE, No. 689/ I —57)

MULTIPLE SPRING MODEL FOR 3D-HYSTERETIC BEHAVIOR OF THIN-WALLED CIRCULAR STEEL PIERS

Lizhi JIANG[1], Yoshiaki GOTO[2] and Makoto OBATA[3]

[1]Graduate Student, Dept. of Civil Eng., Nagoya Institute of Technology
(Gokiso-cho, Showa-ku, Nagoya 466-8555, Japan)
[2]Member of JSCE, Dr. Eng., Professor, Dept. of Civil Eng., Nagoya Institute of Technology
(Gokiso-cho, Showa-ku, Nagoya 466-8555, Japan)
[3]Member of JSCE, Ph. D., Associate Professor, Dept. of Civil Eng., Nagoya Institute of Technology
(Gokiso-cho, Showa-ku, Nagoya 466-8555, Japan)

We propose a hysteretic model of thin-walled circular steel piers under biaxial bending to predict the ultimate seismic behavior of cantilever-type thin-walled circular steel piers. The proposed pier model consists of a concentrated mass and a rigid bar with multiple nonlinear springs located at the pier base. This multiple spring model is characterized by the point that the hysteretic constitutive relation for each spring is determined by the in-plane behavior of steel piers. Herein, the in-plane behavior of the steel piers is predicted by the existing 2-parameter model. The validity of the proposed model is examined by comparing with the results of the 3D-earthquake response analysis, using FEM shell models.

Key Words: *multiple spring, inelastic behavior, local buckling, thin-walled pier, dynamic response analysis*

1. INTRODUCTION

Thin-walled steel piers are often used in Japan as elevated highway bridge piers because of their structural advantages, *i.e.*, small cross-sectional area and high earthquake resistance. In the design of these piers, however, the effects of local buckling on their ductility must be carefully considered, as observed in the 1995 Kobe Earthquake[1] (**Fig.1**). Since the 1995 Kobe Earthquake, much experimental and analytical research[2] has been conducted to examine the stability and ductility of thin-walled steel piers under cyclic loading. Based on these research, some single degree of freedom empirical models such as bi-linear kinematic hardening model[3], 2-parameter model[4] and damage index model[5] have been presented to express the in-plane hysteretic behaviors of steel piers in view of the application to the seismic design based on the dynamic response analysis. Since the bi-linear kinematic hardening model ignores the softening behavior due to local buckling, the application of this model is restricted to the region where the local buckling is insignificant. Regarding the other two models[4), 5)], the empirical formulas have been deduced from a lot of experiments and/or FEM analysis results in order to include the

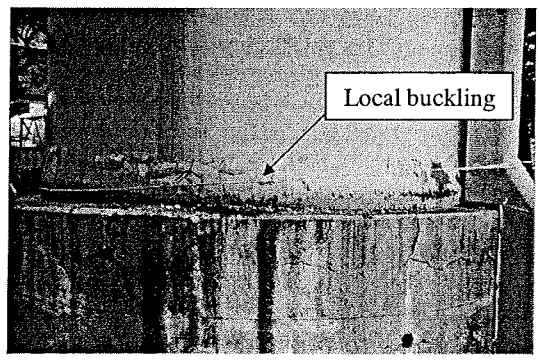

Fig.1 Local buckling of a cylindrical pier in the 1995 Kobe Earthquake

complicated effects of local buckling and cyclic hardening of steel on the hysteretic behavior of piers. The accuracy of these two models is confirmed by the pseudo-dynamic tests under in-plane strong earthquake excitations[4].

Up to the present, the research work concerning the hysteretic modeling of the steel piers has been mainly restricted to their in-plane behaviors. As observed in the 1995 Kobe Earthquake and the recent experiment[6], however, three-dimensional seismic excitations affect the damage of steel piers. Therefore, it is more desirable to consider the three-dimensional effect in design. For this purpose, it is necessary to develop a three-dimensional hysteretic model that considers the interaction of axial force and bi-axial bending.

Herein, as a three-dimensional hysteretic model for thin-walled circular steel piers, we propose a multiple spring model. This model consists of a concentrated mass and a rigid bar with multiple nonlinear springs located at the pier base. The idea of the multiple spring model is similar to that of the four spring model presented by Lai *et al.*[7] that has been used to express the three-dimensional behavior of reinforced concrete elements, although an elastic bar is used in lieu of the rigid bar. Wada *et al.*[8] also presented a multiple shear spring model for reinforced concrete columns where the number of springs is increased compared with the four spring model and the rigid bar is introduced instead of the elastic bar, similar to our model. But his method to determine the spring parameters is not described in detail and looks very empirical. Recently, Ohi *et al.*[9] developed a four spring model for the steel frames by using the multi-linear skeleton line for spring and introducing a target point concept for the hysteretic rule following the original four spring model[7]. However the calibration of spring parameters is based on the monotonic loading test data due to the lack of the suitable data concerning the hysteretic behavior. Furthermore, the method of determining spring parameters is empirical. Four springs are insufficient to express the homogeneous behavior of circular steel piers in any horizontal directions. Here, we determine the number of springs by examining whether the horizontal homogeneous behavior is ensured. What is most important for the multiple spring model is to determine the constitutive rule for each spring so that the effects of local buckling and cyclic strain hardening along with the $P-\Delta$ effect can be properly considered. In our model all the springs are assumed to have the same constitutive relations. These constitutive relations are determined by using curve-fitting techniques such that the multiple spring model can best express the in-plane hysteretic behavior of circular steel piers expressed by the existing 2-parameter model.

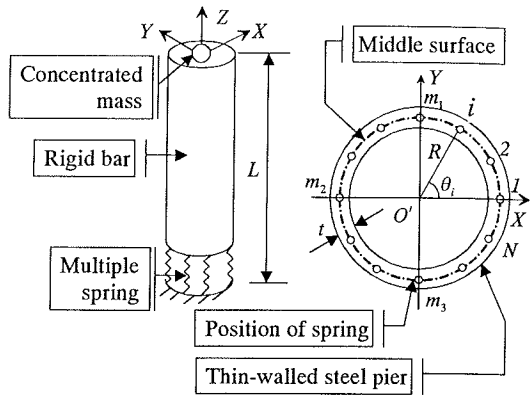

Fig.2 Multiple spring model

The accuracy of our multiple spring model is examined by comparing with the 3-D earthquake response analysis results obtained by geometrically and materially nonlinear FEM shell elements[10]. In this FEM analysis, the three-surface model[11] is used as a cyclic plasticity constitutive model for steel. The proposed multiple spring model is intended to express the hysteretic behavior of thin-walled circular steel piers with constant cross-section. However, as long as the localized deformation occurs in a single location, some minor modification may make it possible to apply the present model to steel piers with variable cross-section.

2. MULTIPLE SPRING MODEL

The pier is modeled by a rigid bar with multiple springs located on the middle surface of the thin-walled circular pier, as illustrated in **Fig.2**. Spring *1* and spring m_2 are located on the X-axis, whilst spring m_1 and spring m_3 are on the Y-axis. It is assumed that no horizontal relative displacement occurs at the base of the pier. Springs are arranged with equal intervals along the middle surface of the thin-walled circular cross-section. Furthermore, the locations of the respective spring are so arranged that they become symmetric with respect to both X and Y axes.

From the kinematic relation, the incremental vertical displacement of the i -th spring Δd_i is expressed as

$$\Delta d_i = -\frac{R}{L}\left(\Delta D_X \cos\theta_i + \Delta D_Y \sin\theta_i\right) + \Delta D_Z \quad (1)$$

where R and L are the radius and height of the pier; ΔD_X , ΔD_Y and ΔD_Z are three incremental translational displacement components at the top of the pier; θ_i is the angle that specifies the location of the i-th spring (**Fig.2**).

The moment equilibrium and the vertical force equilibrium at the base of the pier lead to

$$\Delta F_X = -\frac{R}{L}\sum_{i=1}^{N}\Delta f_i \cos\theta_i \tag{2}$$

$$\Delta F_Y = -\frac{R}{L}\sum_{i=1}^{N}\Delta f_i \sin\theta_i \tag{3}$$

$$\Delta F_Z = \sum_{i=1}^{N}\Delta f_i \tag{4}$$

where ΔF_X , ΔF_Y and ΔF_Z are three incremental force components applied at the top of the pier; Δf_i is the incremental force of the i-th spring and N is the total number of springs.

For each spring, the following constitutive relation holds.

$$\Delta f_i = k_i \Delta d_i \tag{5}$$

where k_i is the tangent stiffness of the i-th spring. From Eqs. (1)~(5), we can get the following relation of the incremental force-displacement relation at the top of the pier,

$$\begin{Bmatrix}\Delta F_X\\ \Delta F_Y\\ \Delta F_Z\end{Bmatrix} = \begin{bmatrix}a_{11} & a_{12} & a_{13}\\ a_{21} & a_{22} & a_{23}\\ a_{31} & a_{32} & a_{33}\end{bmatrix}\begin{Bmatrix}\Delta D_X\\ \Delta D_Y\\ \Delta D_Z\end{Bmatrix} \tag{6}$$

where

$$a_{11} = \frac{R^2}{L^2}\sum_{i=1}^{N} k_i \cos^2\theta_i \tag{7}$$

$$a_{12} = a_{21} = \frac{R^2}{L^2}\sum_{i=1}^{N} k_i \cos\theta_i \sin\theta_i \tag{8}$$

$$a_{13} = a_{31} = -\frac{R}{L}\sum_{i=1}^{N} k_i \cos\theta_i \tag{9}$$

$$a_{22} = \frac{R^2}{L^2}\sum_{i=1}^{N} k_i \sin^2\theta_i \tag{10}$$

$$a_{23} = a_{32} = -\frac{R}{L}\sum_{i=1}^{N} k_i \sin\theta_i \tag{11}$$

$$a_{33} = \sum_{i=1}^{N} k_i \tag{12}$$

3. CONSTITUTIVE MODEL FOR EACH SPRING

(1) General

In the multiple spring model, it is critically important to determine the constitutive relation for springs so that the model can properly express the effects of local buckling and cyclic strain hardening along with the $P-\Delta$ effect. In our model all the springs are assumed to have the same constitutive relation.

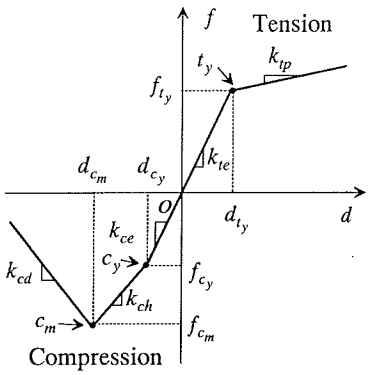

Fig.3 Skeleton curve of spring

The local buckling occurs only in the location where the axial compressive stress becomes dominant. Therefore, the softening behavior of a spring is considered only on the compression side. The shape of the skeleton curve adopted here is shown in **Fig.3**. The tension side of the skeleton curve is expressed by the bi-linear curve while the compression side is by the tri-linear one with a descending part that represents the strength deterioration due to local buckling. In determining the model parameters for the skeleton curve of the spring, we use two-step process. First, we assume that the tension side of the skeleton curve is the same as the compression side. Then, the model parameters are determined by curve fitting technique, using the FEM results with beam elements where the local buckling effects are ignored. Second, the compression side is determined on the basis of the 2-parameter model's empirical in-plane skeleton curve[4] that takes into account the local buckling effect.

As for the hysteretic rule for each spring, we adopt the basic idea of the 2-parameter model and present a new hysteretic rule.

(2) Determination of tension side of skeleton curve

The skeleton curve of a spring (**Fig.3**) reflects the behavior of piers. When some parts of pier are subjected to axial tensile stress, local buckling will not occur in these parts. So the tension side of skeleton curve is assumed to be bi-linear type without considering buckling. To determine the parameters of the bi-linear model, we use monotonic

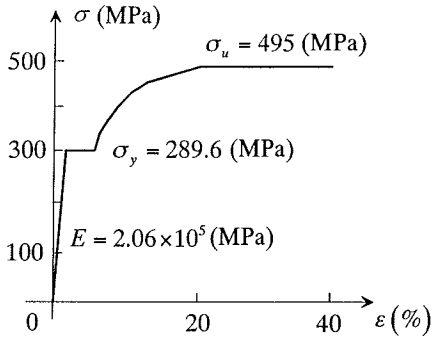

Fig.4 Uniaxial stress-strain relation for steel SS400

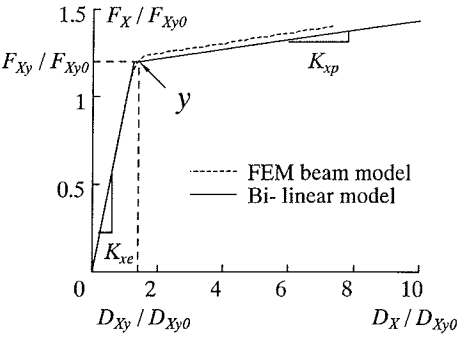

Fig.5 Bi- linear model of column

in-plane horizontal force-displacement relation at the top of the pier that is given by FEM analysis with beam element. In such FEM analysis, local buckling effects are excluded but the material nonlinearity of steel is considered by the uniaxial constitutive model of steel as shown in **Fig.4**. For simplicity, the vertical force is assumed to be zero and only the horizontal force is applied. This assumption is valid since the geometrical nonlinearity due to the $P-\Delta$ effect is taken into account when we determine the compression side of the skeleton curve as explained later in **3. (3)**.

From the analysis results of several piers, it is found that the horizontal force-displacement relation at the top of pier can be well approximated by a bi-linear curve, as illustrated in **Fig.5**, where the intersection point y of the two sublines are given in the following

$$F_{Xy} = 1.2F_{Xy0} = 1.2\frac{\sigma_y I}{L(R+\frac{t}{2})} \tag{13}$$

$$D_{Xy} = 1.2D_{Xy0} = 1.2\frac{F_{Xy0}}{K_{xe}} \tag{14}$$

where F_{Xy0} and D_{Xy0} are yield horizontal force and yield horizontal displacement of pier without vertical force obtained by the beam model; σ_y is the yield stress of steel; I is the second moment of inertia; L is the height of the pier; R and t are the radius and the thickness, respectively, of the thin-walled circular steel pier; K_{xe} that is the initial elastic stiffness is given as

$$K_{xe} = \frac{1}{\frac{L^3}{3EI}+\frac{L}{GA\kappa}} \tag{15}$$

where G, A and κ are the shear elastic modulus, cross-sectional area and shear coefficient respectively, of the thin-walled circular steel piers. The secondary tangent stiffness is

$$K_{xp} = 0.04K_{xe} \tag{16}$$

The coefficients 1.2 and 0.04 in Eqs. (13), (14) and (16) are determined based on the results of our FEM analyses by ABAQUS[10]. These values are identified in the present research.

Finally, the monotonic horizontal force-displacement relation of the pier with beam model is expressed as

$$F_X = \begin{cases} K_{xe}D_X & \left(0 \le D_X \le D_{Xy}\right) \\ F_{Xy} + K_{xp}\left(D_X - D_{Xy}\right) & \left(D_{Xy} < D_X\right) \end{cases} \tag{17}$$

Based on the force-displacement curve of the pier expressed by Eq. (17), the parameters of the skeleton curve on the tension side of the spring model (**Fig.3**) are obtained. Herein, the horizontal force is applied in the X direction. From Eq. (6), the incremental in-plane (X-Z plane) force-displacement relations are derived respectively as

$$\Delta F_X = a_{11}\Delta D_X + a_{13}\Delta D_Z \tag{18}$$

$$\Delta F_Z = a_{13}\Delta D_X + a_{33}\Delta D_Z = 0 \tag{19}$$

When we determine the elastic constant k_{te} of the spring, k_i can be taken as constant, that is, $k_i = k_{te}$. Furthermore, a fully plastic state can be assumed to determine k_{tp}, because the monotonic horizontal force-displacement relation is approximated by the bilinear curve where the secondary line corresponds to the fully plastic state. Therefore, in both cases to determine stiffness k_{te} and k_{tp}, k_i can be assumed constant and Eqs. (18) and (19) can be rewritten as

$$\Delta F_X = kb_{11}\Delta D_X - kb_{13}\Delta D_Z \tag{20}$$

$$\Delta F_Z = -kb_{31}\Delta D_X + kb_{33}\Delta D_Z = 0 \tag{21}$$

where k is the tangent stiffness of the springs that

becomes k_{te} in the elastic range and k_{tp} in the plastic range; $b_{11} = \frac{R^2}{L^2}\left(\sum_{i=1}^{N}\cos^2\theta_i\right)$; $b_{13} = b_{31} = \frac{R}{L}\left(\sum_{i=1}^{N}\cos\theta_i\right)$ and $b_{33} = N$. It should be noted that $\sum_{i=1}^{n}\cos\theta_i = 0$ when the springs are located symmetrically with respect to the Y-axis. Therefore, Eqs. (20) and (21) are reduced to

$$\Delta F_X = kb_{11}\Delta D_X \tag{22}$$

$$\Delta D_Z = 0 \tag{23}$$

Eq. (22) is used to determine two of the parameters of spring: the elastic tangent stiffness k_{te} and the plastic tangent stiffness k_{tp}

$$k_{te} = \frac{K_{xe}}{b_{11}} \tag{24}$$

$$k_{tp} = \frac{K_{xp}}{b_{11}} \tag{25}$$

The intersection point t_y (d_{t_y}, f_{t_y}) of the two sublines of the bi-linear spring model on tension side is determined by a trial and error method such that the final elasto-plastic range of monotonic loading curve by multiple spring model may coincide well with the bi-linear horizontal force-displacement curve of a pier determined by FEM beam analysis as shown in **Fig.5**.

If we assume a value of d_{t_y} , a monotonic horizontal force-displacement curve can be calculated by the multiple spring model. **Fig.6** shows a comparison between the bi-linear model and the horizontal force-displacement curve obtained by the multiple spring model. It is observed from **Fig.6** that the stiffness of monotonic loading curve by the multiple spring model decreases gradually after yielding and approaches to a final value corresponding to a fully plastic state. $a\,(D_{Xa}, F_{Xa})$ is a point on the secondary line of the bi-linear model of a pier. $as\,(D_{Xas}, F_{Xas})$ is a point on the monotonic horizontal force-displacement curve by the multiple spring model, where $D_{Xas} = D_{Xa}$. D_{Xa} is a relatively large value that represents almost a fully plastic state. As illustrated in **Fig.6**, the optimum value of d_{t_y} exists somewhere between $d_{t_{yl}}$ and $d_{t_{yr}}$. The following can be given as initial limiting values for the bisection iterative method:

$$d_{t_{yl}} = 0 \tag{26}$$

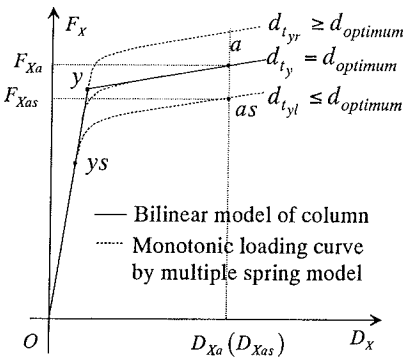

Fig.6 Determination of tension side of skeleton curve

$$d_{t_{yr}} = \frac{R}{L}D_{Xy} \tag{27}$$

where D_{Xy} is the horizontal coordinate of the intersection point y of the bi-linear pier model as shown in **Fig.5**. Eq. (27) corresponds to the displacement of the outermost springs when the horizontal displacement at the top of the pier reaches D_{Xy} . As is clear from the bi-linear approximation shown in **Fig.5**, the yielding of multiple spring model starts at the outermost springs under the horizontal displacement smaller than D_{Xy} . Thus, $d_{t_y} < \frac{R}{L}D_{Xy}$. Once the initial range of d_{t_y} is identified, the usual bisection iterative method is used to determine the optimum value of d_{t_y} . After d_{t_y} is obtained, f_{t_y} is given by

$$f_{t_y} = k_{te}d_{t_y} \tag{28}$$

The tension side of the skeleton curve is finally determined as

$$f = \begin{cases} k_{te}d & ,\left(0 \leq d < d_{t_y}\right) \\ f_{t_y} + k_{tp}\left(d - d_{t_y}\right), & \left(d_{t_y} \leq d\right) \end{cases} \tag{29}$$

(3) Determination of compression side of skeleton curve

After the tension side of the skeleton curve is determined, we proceed to identify the compression side. Herein, the empirical in-plane skeleton curve of the 2-parameter model[4] illustrated in **Fig.7** is used as a basis for our curve fitting. The 2-parameter model is an evolutionary-degrading restoring force model developed for thin-walled steel bridge piers. In this model the following three non-dimensional quantities[12] are used as governing parameters for

thin-walled circular steel piers: the radius-to-thickness ratio parameter R_t ; the slenderness ration parameter λ and axial force ratio μ.

$$R_t = \frac{R}{t}\frac{\sigma_y}{E}\sqrt{3(1-\nu^2)} \tag{30}$$

$$\lambda = \frac{2L}{r}\frac{1}{\pi}\sqrt{\frac{\sigma_y}{E}} \tag{31}$$

$$\mu = \frac{P}{\sigma_y A} \tag{32}$$

where R and t are the radius and the thickness, respectively; σ_y is the yield stress of steel; E is the Young's modulus; ν is the Poisson's ratio; L is the height of the pier and r is the radius of gyration of the cross-section; P is a constant vertical compressive load acting on the top of the pier; A is the cross-sectional area of the pier.

As can be seen from **Fig.7**, the skeleton curve of the 2-parameter model is uniquely determined by the yield point y (D_{Xy} , F_{Xy}), the maximum point $m(D_{Xm}, F_{Xm})$ and the softening stiffness K_d. The details of how to determine these quantities in terms of the governing parameters R_t , λ and μ are explained in Refs. 4), 12) and 13). Here we only show the parameters of this model

$$\frac{F_{Xm}}{F_{Xy}} = \frac{0.02}{(R_t\lambda)^{0.8}} + 1.10 \tag{33}$$

$$\frac{D_{Xm}}{D_{Xy}} = \frac{1}{3\left(R_t\lambda^{0.5}\right)^{0.8}} - \frac{2}{3} \tag{34}$$

$$\frac{K_d}{K_1} = -1.41R_t(1+\mu)^5\lambda^{1.3} \tag{35}$$

where F_{Xy} , D_{Xy} and K_1 are obtained from the elastic theory.

Based on the 2-parameter model, we now try to determine the parameters of the tri-linear skeleton curve concerned with the compressive behavior of the spring as shown in **Fig.3**. The skeleton curve of the spring under compressive force is composed of elastic line, hardening line and descending line. The tangent stiffness of the three lines are expressed by k_{ce} , k_{ch} and k_{cd} . Two intersection points of the tri-linear curve is denoted by c_y (d_{c_y}, f_{c_y}) and c_m (d_{c_m}, f_{c_m}). Among these parameters, five are independent and must be determined.

The stiffness of the elastic line can be assumed to be the same as the tension side

$$k_{ce} = k_{te} \tag{36}$$

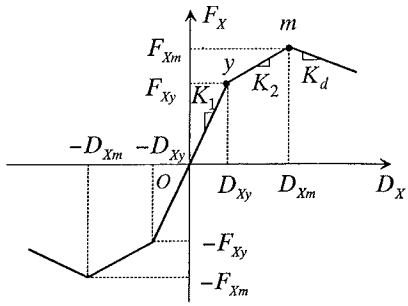

Fig.7 Skeleton curve of 2-parameter model

It may be assumed that the yield point y (F_{Xy}, D_{Xy}) of the pier skeleton curve approximately corresponds to the state when the outermost spring on the compression side reaches the yield deformation d_{c_y}.

Eq. (1) is integrated with respect to the spring *1* as

$$d_1 = -\frac{R}{L}D_X\cos\theta_1 + D_Z \tag{37}$$

Noting that $d_1 = d_y$, $D_X = D_{Xy}$, $\cos\theta_1 = 1$ and $D_Z = -PL/(EA)$, the yield point of the compression side is given by

$$d_{c_y} = -\frac{R}{L}D_{Xy} - \frac{PL}{EA} \tag{38}$$

$$f_{c_y} = k_{ce}d_{c_y} \tag{39}$$

The three parameters: d_{c_m} , k_{ch} (or f_{c_m}) and k_{cd} are determined by a trial and error method. If we assume reasonable values for these three parameters, we can calculate a monotonic loading curve as shown in **Fig.8** by the multiple spring model. y is the yield point and m is the peak point of the tri-linear skeleton curve of the 2-parameter model. ms is the peak point obtained by the multiple spring model. The pier under deformation of D_{Xp} is in a state where the pier exhibits a steady softening behavior. In this state, the compressive springs are in the fully softening state and the tensile springs are in the fully plastic state. We will determine the set of values d_{c_m} , k_{ch} and k_{cd} so that the point ms and the final descending line stiffness K_{ds} matches with the point m and K_d , respectively.

At the fully softening stage when $D_X = D_{Xp}$, K_{ds} is only governed by k_{cd} . Thus, the value of k_{cd} is first determined. In determining k_{cd} what is needed for d_{c_m} and k_{ch} is just to give them a set of reasonable values, not exact values. The following

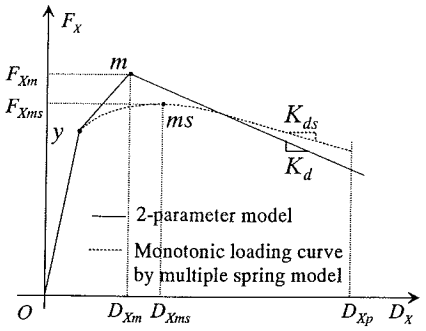

Fig.8 Fitting of multiple spring model to 2-parameter model in terms of softening stiffness

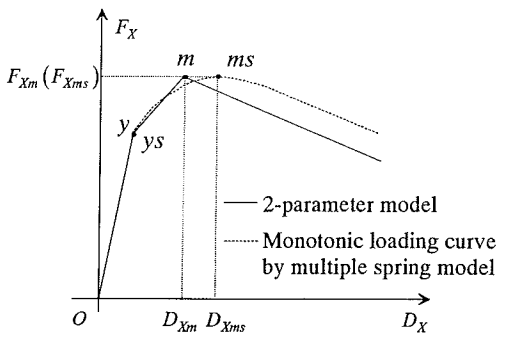

Fig.9 Fitting of multiple spring model to 2-parameter model in terms of peak point

equations are used to predict the reasonable values.

$$d_{c_m} = -\frac{R}{L} D_{Xm} \tag{40}$$

$$k_{ch} = \frac{k_{ce}}{2} \tag{41}$$

Eq. (40) corresponds to the displacement of the outermost springs when the horizontal displacement at the top of the pier reaches D_{Xm}, while, just as a reasonable value, the effect of constant vertical force P on horizontal displacement is neglected. As shown in Eq. (41), half of the initial elastic stiffness k_{ce} is given to k_{ch} as a reasonable value. Once reasonable values are given to d_{c_m} and k_{ch}, k_{cd} is determined by the usual bisection method.

If we express the range of k_{cd} as $k_{cdl} < k_{cd} < k_{cdr}$, the limiting values for the bisection method can be assumed as

$$k_{cdl} = C_1 \tag{42}$$

$$k_{cdr} = 0 \tag{43}$$

where C_1 is a big negative value.

Secondly, the two parameters, point c_m (d_{c_m}, f_{c_m}) or (d_{c_m}, k_{ch}) can also be determined by the bisection method for two variables. Herein, d_{c_m} and k_{ch} are selected as these two variables to be identified. Since a particular technique is included in the bisection method for two variables, the method is explained in some detail.

The ranges for the two parameters are denoted here as $d_{c_{ml}} < d_{c_m} < d_{c_{mr}}$ and $k_{chl} < k_{ch} < k_{chr}$. The initial value for $d_{c_{ml}}$ can be given as

$$d_{c_{ml}} = -\frac{R}{L} D_{Xm} - \xi \frac{PL}{EA} \tag{44}$$

where ξ is a constant that reflects the effect of plastification on the axial deformation. It is found that $\xi = 2.$ is acceptable in analyses.

If we use $d_{c_{ml}}$ given by Eq. (44) as d_{c_m} in the skeleton curve of the spring model, the outermost spring on compression side of the multiple spring model starts to enter the descending line when the horizontal displacement approaches D_{Xm}. Under this displacement, however, the rest of the springs on the compression side are still in the hardening stage. Therefore, under D_{Xm}, the peak point ms for the multiple spring model is not reached yet. This implies that $D_{Xms} > D_{Xm}$. As can be seen from **Fig.9**, if we adopt d_{c_m} that satisfies the relation $D_{Xms} > D_{Xm}$, it is possible to determine the value of k_{ch} that ensures $F_{Xms} = F_{Xm}$. So, in the two-variable bi-section method, we can choose $d_{c_{ml}}$ as an initial value of d_{c_m} and increase $d_{c_{ml}}$ with a small step increment with keeping $F_{Xms} = F_{Xm}$ until $D_{Xms} < D_{Xm}$ is satisfied. The trial value of d_{c_m} in the i-th iterative process is given as

$$d_{c_m}^{(i)} = d_{c_{ml}} + i\Delta d_{c_{ml}} \tag{45}$$

where $\Delta d_{c_{ml}}$ can be set as

$$\Delta d_{c_{ml}} = -0.005 d_{c_{ml}} \tag{46}$$

For a given $d_{c_m}^{(i)}$, the usual bisection iterative method is used to determine a corresponding hardening stiffness $k_{ch(i)}$. The initial range for $k_{ch(i)}$ may be assumed as

$$k_{chl(i)} = 0 \tag{47}$$

$$k_{chr(i)} = k_{ce} \tag{48}$$

The trial value for the j-th iterative process for $k_{ch(i)}$

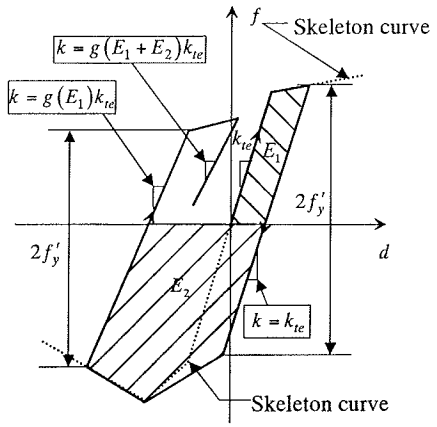

Fig.10 Stiffness degradation and shrinkage of elastic range in spring model

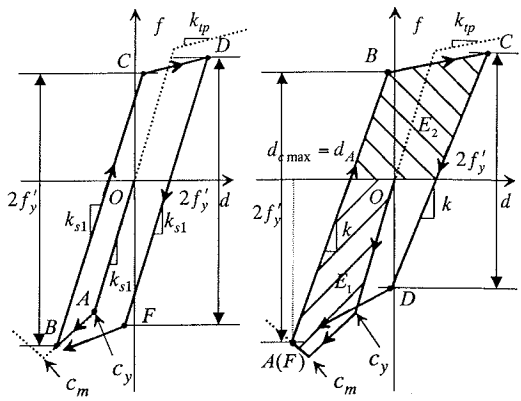

(a) Unloading and reverse loading in the hardening range (case 1)

(b) Unloading and reverse loading in the degrading range (case 2)

Fig.11 Hysteretic rule for spring model

is determined by

$$k_{ch(i)}^{(j)} = \frac{k_{chl(i)} + k_{chr(i)}}{2} \tag{49}$$

With the parameters so assumed, point $ms(D_{Xms(i)}^{(j)}, F_{Xms(i)}^{(j)})$ can be calculated by the multiple spring model. If $F_{Xms(i)}^{(j)} > F_{Xm}$, then we set $k_{chl(i)} = k_{ch(i)}^{(j)}$. Otherwise, $k_{chr(i)} = k_{ch(i)}^{(j)}$. This iterative process for a given $d_{c_m}^{(i)}$ is continued until the following tolerance is satisfied

$$\frac{\left|F_{Xms(i)}^{(j)} - F_{Xm}\right|}{\left|F_{Xm}\right|} \le \varepsilon_3 \tag{50}$$

After the optimum value of k_{ch} is obtained for $d_{c_m}^{(i)}$, we proceed to identify the optimum value of k_{ch} for the $d_{c_m}^{(i+1)}$ given by Eq. (45).

The above process is repeated until $D_{Xms} < D_{Xm}$ is first satisfied for $d_{c_m}^{(i+1)}$. Then, we can identify the range for d_{c_m} as

$$d_{c_{ml}} = d_{c_m}^{(i)} \tag{51}$$

$$d_{c_{mr}} = d_{c_m}^{(i+1)} \tag{52}$$

Once the range of d_{c_m} is identified, the next trial value $d_{c_m}^{(i+2)}$ is given by the usual bi-section method instead of Eq. (45) as

$$d_{c_m}^{(i+2)} = \frac{d_{c_{ml}} + d_{c_{mr}}}{2} \tag{53}$$

After the optimum value of k_{ch} is obtained for the given $d_{c_m}^{(i+2)}$, $D_{Xms}^{(i+2)}$ is calculated by using k_{ch} and $d_{c_m}^{(i+2)}$. The optimum value of $d_{c_{ml}}$ is determined by the condition that the following tolerance is satisfied

$$\frac{\left|D_{Xms}^{(i+2)} - D_{Xm}\right|}{D_{Xm}} \le \varepsilon_4 \tag{54}$$

Finally, the skeleton curve on the compression side is determined as

$$f = \begin{cases} k_{ce} d & ,\left(d_{c_y} \le d \le 0\right) \\ f_{c_y} + k_{ch}\left(d - d_{c_y}\right) & ,\left(d_{c_m} < d < d_{c_y}\right) \\ f_{c_m} + k_{cd}\left(d - d_{c_m}\right) & ,\left(d \le d_{c_m}\right) \end{cases} \tag{55}$$

(4) Hysteretic rule

The hysteretic rule of the spring model is divided into two parts, that is, the compression side and the tension side.

Regarding the rule on the compression side, the one similar to the 2-parameter model is utilized. This is because the skeleton curve of the spring model on the compression side is represented by the tri-linear curve given by the 2-parameter model. The hysteretic behavior of the 2-parameter model are characterized by the three rules: 1) the whole loading history is divided into two stages to consider the cyclic hardening effect; 2) the accumulated hysteretic energy of pier is used to predict the stiffness degradation; 3) the maximum deformation is used as an index to consider the strength degradation.

Regarding the hysteretic rule on the tension side, however, the skeleton curve of the spring model is

expressed by a bi-linear curve without descending line, being different from the 2-parameter model. Therefore, we adopt the kinematic hardening rule on the tension side and the hardening rule with negative stiffness on the compression side. The details of these rules are explained below.

Following the original 2-parameter model, the loading history of the spring model on the compression side is classified into two stages: hardening stage and degrading stage. Hardening stage is defined by the condition that the deformation of a spring d is within the range specified by $d_{c_m} \le d$. d_{c_m} is the displacement at the peak point of the skeleton curve on the compression side. In this stage, the behavior of spring is characterized by the cyclic hardening behavior where the elastic range and the elastic stiffness stay constant. Once the displacement passes d_{c_m}, then the spring moves into the degrading stage. The hysteretic behavior in the degrading stage is characterized by the deterioration of the elastic stiffness k and the shrinkage of elastic range $2f_y'$, as illustrated in **Fig.10**.

As for the degradation rule for elastic stiffness k, the idea of the 2-parameter model is used for each spring. In the degrading stage, stiffness degradation occurs, whenever unloading occurs. The degraded elastic stiffness k is assumed to be governed as follows by the accumulated hysteretic energy of the spring, $\sum E_i$.

$$\frac{k}{k_{te}} = 1 - \frac{1}{\alpha}\ln\left(\frac{\sum E_i/E_e}{100} + 1\right) = g\left(\sum E_i\right) \qquad (56)$$

where $\alpha = 1/(7.36R_t)$ according to the 2-parameter model. Although the shapes of skeleton curves on the tension side and compression side are different, we use the same value for the empirical parameter α.

With the use of the degraded elastic stiffness k calculated by Eq. (56), the shrinked elastic range $2f_y'$ is assumed to be given by

$$2f_y' = k(d_{t_y} + d_{c_y}) \qquad (57)$$

where d_{t_y} and d_{c_y} denote yield displacements of the skeleton curve on the tension side and the compression side, respectively. The above equation implies that the elastic range shrinks in proportion to the elastic stiffness.

In what follows, two important loading histories are chosen to explain the hysteretic rules. The first one represents the loading history in the hardening stage, while the second one represents the loading history in the degrading stage.

Fig.11(a) illustrates the hysteretic rule when the spring is in the hardening stage and the unloading first occurs on the compression side. At this stage the cyclic hardening effect is the major characteristics of the hysteretic behavior. Starting from point O, the initial yielding occurs at point A. Then, the loading point follows a hardening line heading to the peak point c_m (d_{c_m}, f_{c_m}). Suppose that unloading occurs at point B on the hardening line and this unloading is followed by reverse loading. The loading point goes to the yield point C on the tension side with the elastic stiffness of k_{s1} that is the same as the initial elastic stiffness. In the hardening stage, the kinematic hardening model is used and the elastic range $2f_y'$ remains constant as given by

$$2f_y' = f_{t_y} + f_{c_y} \qquad (58)$$

where f_{t_y} and f_{c_y} denote yield forces of the skeleton curve on tension side and compression side, respectively. Beyond point C, the loading point follows the hardening line that is parallel to the initial skeleton curve where the stiffness of the hardening line on the tension side keeps the initial value k_{tp}. If unloading occurs at point D, the loading point heads to the yield point F, where both the elastic stiffness k and the elastic range $2f_y'$ keep the initial values. After point F the loading point will again follows a hardening line heading to the peak point c_m (d_{c_m}, f_{c_m}).

Fig.11(b) shows the case when the first unloading occurs at point A in the degrading range on the compression side. From point A, the loading point goes to the yield point B under unloading and subsequent reverse loading. Since the loading point is in the degrading range, the elastic stiffness k decreases and the elastic range $2f_y'$ shrinks, depending on the hysteretic energy E_1, as respectively given by Eqs. (56) and (57). After point B is reached, the loading point follows a hardening line that is parallel to the skeleton curve with the stiffness of k_{tp}. When unlading occurs at point C, loading point goes to the yield point D under reverse loading. In this elastic stage, the elastic stiffness and the elastic range are governed by the accumulated hysteretic energy $E_1 + E_2$. After point D is reached, the loading point heads to point F that is on the skeleton curve with the deformation of $d_{c\max}$. $d_{c\max}$ denotes the maximum deformation that the spring has ever experienced on the compression side.

Table 1 Dimensions and governing parameters of circular pier models

Pier model	L (m)	R (m)	t (m)	R_t	λ	μ	Mass (kg)	Number of springs
1	14.814	1.00	0.0332	0.07	0.5	0.10	8.174×10^5	32
2	19.997	1.35	0.0285	0.11	0.5	0.10	9.530×10^5	32
3	11.851	1.00	0.0332	0.07	0.4	0.15	9.343×10^5	32

Table 2 Identified parameters for the skeleton curve of spring

Pier model	1	2	3
k_{tp} (MPa)	7.41	6.38	9.14
k_{te} (MPa)	265	228	326
k_{ce} (MPa)	265	228	326
k_{ch} (MPa)	22.6	140.	15.0
k_{cd} (MPa)	-41.6	-52.5	-48.5
d_{t_y} (m)	0.00618	0.00840	0.00502
f_{t_y} (MN)	1.64	1.91	1.64
d_{c_y} (m)	-0.00702	-0.00953	-0.00570
f_{c_y} (MN)	-1.86	-2.17	-1.86
d_{c_m} (m)	-0.0176	-0.0116	-0.0151
f_{c_m} (MN)	-2.10	-2.46	-2.00

Table 3 Three-surface model parameters

Steel Type	Parameters
SS400	E =206.0 (GPa) σ_y =289.6 (MPa) σ_u =495.0 (MPa) ν =0.3 ε^0_{yp} =0.0183 f_b/σ_y =0.581 β =100 ρ =2 H_{dci}/E =0.05 H^p_{mon} : (*)

(*): Plastic modulus determined by monotonic loading test[11].

Table 4 Comparison of computation time

Pier model	Input wave	Number of nodes in FEM shell model	Time ratio (Multiple spring model : FEM shell model)
1	HKB (15sec.)	2940	1 : 5040
1	JMA (15sec.)	2940	1 : 6480
2	JMA (10sec.)	3360	1 : 5760
3	JMA (15sec.)	2640	1 : 5040

The validity of the present hysteretic rules is examined in the next section, by comparing the hysteretic curves of steel piers obtained by the multiple spring model with those by the 2-parameter model.

4. COMPARISONS WITH THE OTHER MODELS

(1) In-plane hysteretic behavior

Herein, we examine the accuracy of the multiple spring model by comparing with 2-parameter model. For this purpose, three pier models with different

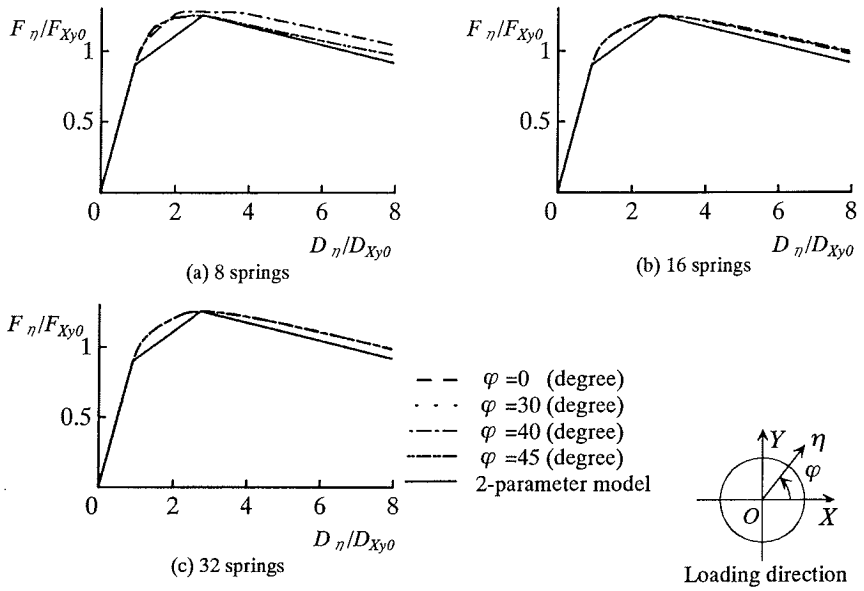

Fig.12 Homogeneity of multiple spring model expressed in terms of horizontal force F_η-horizontal displacement D_η relation (pier 1)

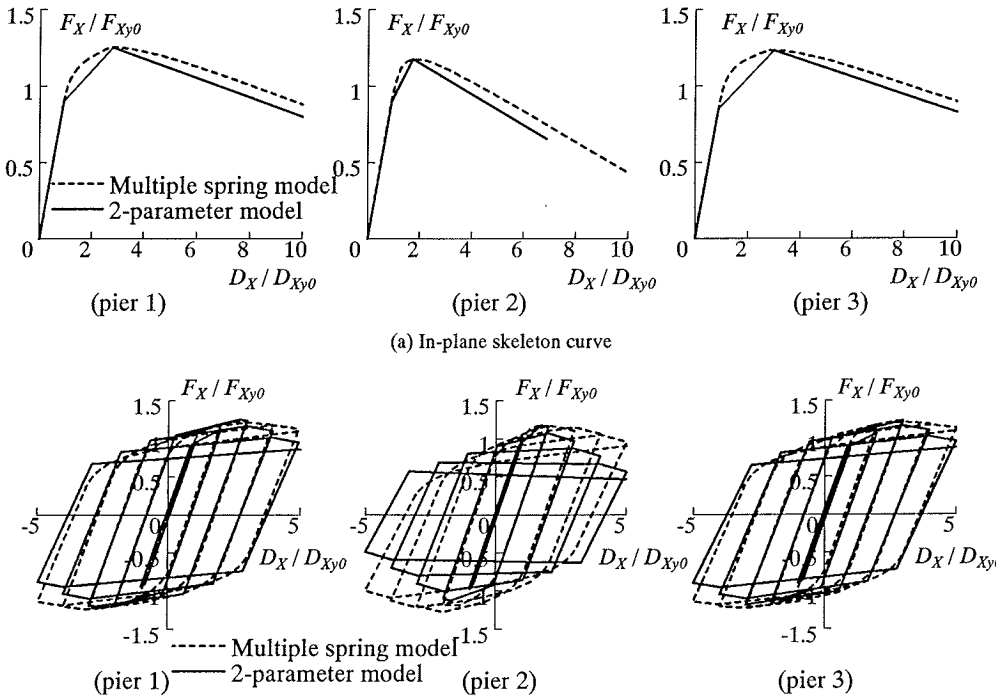

(a) In-plane skeleton curve

(b) In-plane hysteretic curve

Fig.13 Comparison between multiple spring model and 2-parameter model

governing parameters shown in **Table 1** are used as numerical examples. Since the 2-parameter model is applicable for thin-walled circular steel piers with $0.07 \le R_t \le 0.11$, pier 1 with $R_t = 0.07$ and pier 2 with $R_t = 0.11$ are adopted here to cover the applicable range for R_t. The other two governing parameters λ and μ are changed for pier 3 with keeping $R_t = 0.07$.

First, the parameters for the skeleton curves of the springs are identified following the procedure explained in section **3** based on the 2-parameter model. Parameters of the skeleton curves so identified are summarized in **Table 2**. The number of springs, that is 32, is determined by considering homogeneous behavior of steel piers in any horizontal directions. In **Fig.12,** it is shown how the horizontal force-horizontal displacement relation of pier 1 becomes homogeneous by increasing the number of springs. From this figure, it is observed that 16 springs are enough to ensure the homogeneity. Herein, 32 springs are used by taking into account of the homogeneous behavior of pier 2 and pier 3.

In **Fig.13**, the multiple spring model is compared with the 2-parameter model for three pier models in terms of the in-plane skeleton curves and hysteretic behaviors. It is observed from **Fig.13**(a) that the multiple spring model shows acceptable accuracy to express the in-plane skeleton curves of the 2-parameter model. However, some difference exists in the cyclic behavior in the post-peak range. This difference is more evident for pier 2 with a larger value of R_t where the deterioration is strongly affected by the local buckling. There still remains some room to improve the hysteretic rule for thinner circular steel piers.

(2) 3-D dynamic response

In the three-dimensional dynamic response analyses, the accuracy of the multiple spring model is examined in comparison with the 3-D FEM dynamic analysis using shell element where the local buckling behavior is precisely considered. Piers shown in **Table 1** with different values of R_t are chosen for these analyses. The FEM analysis using shell elements is carried by ABAQUS[10]. The pier model used for the FEM analysis is illustrated in **Fig.14**. The thick shell element S4R is chosen as the element type in the whole cylinder. The very fine mesh division is used especially near the pier base where large localized deformation is expected to occur. As the constitutive model to express the cyclic plasticity of steel, the three-surface model[11] is implemented in ABAQUS by using the user defined subroutine

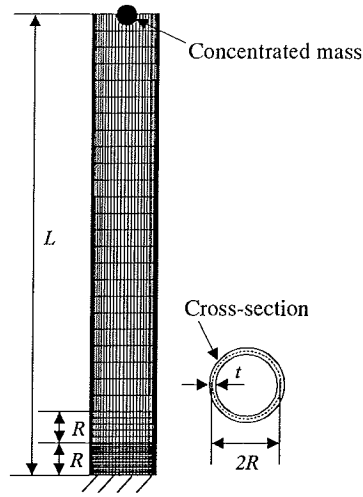

Fig.14 Pier model for dynamic analysis

feature. The material constants of the three-surface model are given in **Table 3**.

Regarding the multiple spring model, number of springs used in the present analysis is the same as that in the previous sub-section **4. (1)**. For pier 1, two kinds of earthquake waves recorded in the 1995 Kobe Earthquake are applied. One is the HKB (Higashi Kobe Bridge) acceleration wave where *L-G*, *T-R* and *U-D* components are assumed to be respectively coincident with *X*, *Y* and *Z* components. The other is the JMA (Japan Meteorological Agency) acceleration wave where *E-W*, *N-S* and *U-D* components are used as *X*, *Y* and *Z* direction. In the analysis of pier 2 and pier 3, only the JMA record is considered. The integration time step used in the 3-D earthquake response analysis is set as 0.005 second for JMA wave and 0.01 second for HKB wave. In **Table 4**, the multiple spring model is compared with the FEM shell model in view of the computational efficiency. It can be seen from **Table 4** that the computation time is drastically shortened by the multiple spring model.

The results of the earthquake response analysis obtained by the multiple-spring model are summarized in **Figs.15~24**, in comparison with those obtained by the FEM analysis. **Figs.15~18** show the sway displacement response histories of piers and **Figs.19~22** illustrate the sway-displacement trajectories. **Fig.24** shows the final deformation patterns of pier models obtained by FEM analysis. From this figure, local buckling patterns are observed in all piers. Among the three piers, pier 3 with the largest radius-to-thickness ratio exhibits the largest localized deformation. This large localized

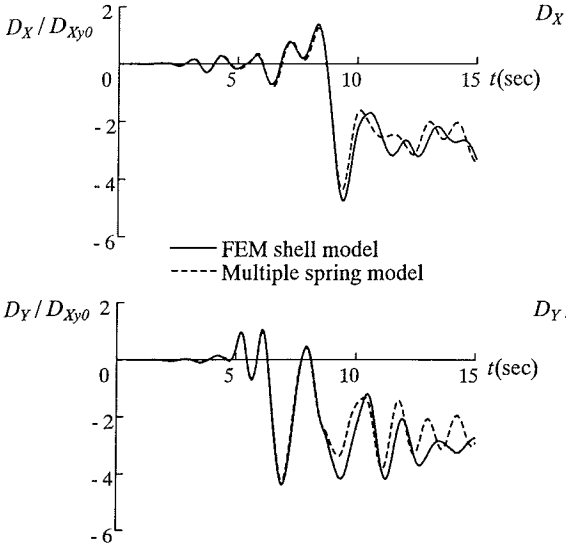

Fig.15 Time horizontal response displacement of pier 1 under HKB wave

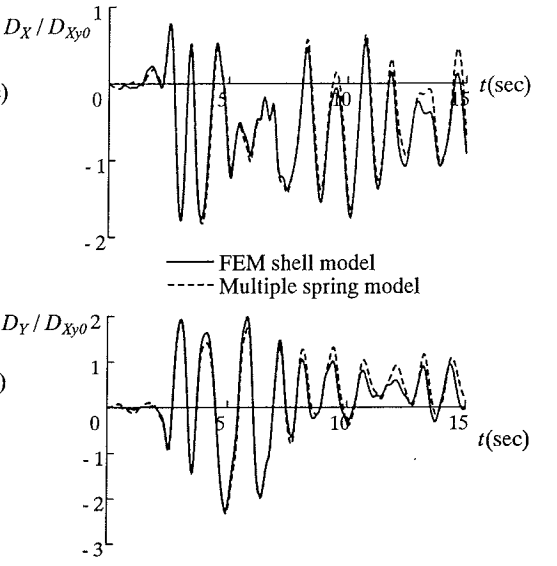

Fig.16 Time- horizontal response displacement of pier 1 under JMA wave

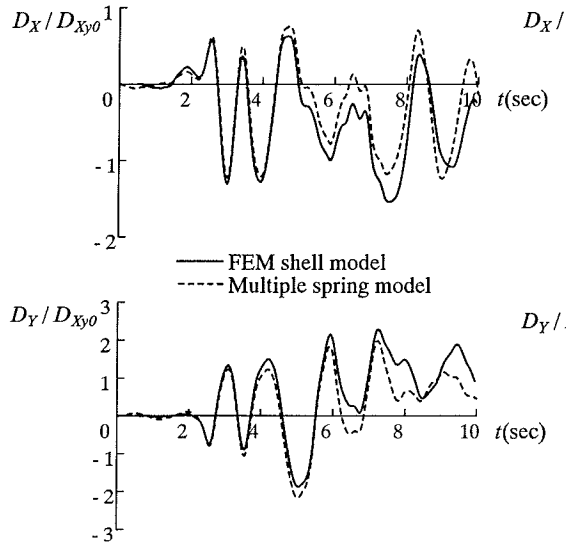

Fig.17 Time- horizontal response displacement of pier 2 under JMA wave

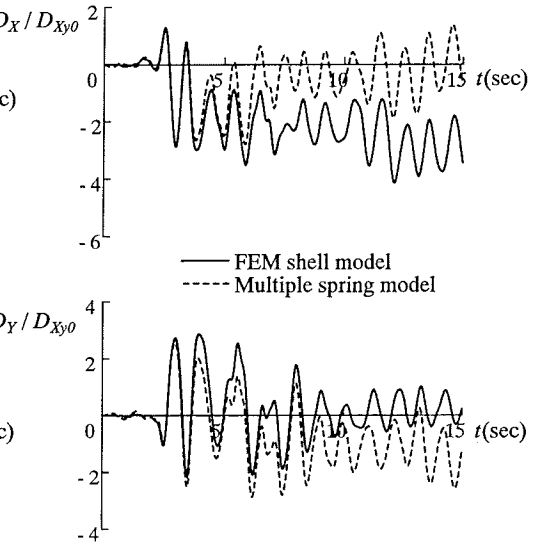

Fig.18 Time- horizontal response displacement of pier 3 under JMA wave

deformation may lead to some discrepancy between the FEM shell model and the multiple spring model in the horizontal response displacement of pier 3, as can be seen from **Figs.13**(b), **18** and **22**. Except for the error caused by highly localized deformation, it is observed from **Figs.15~18** and **Figs.19~22** that the proposed multiple spring model can be an acceptable alternative to the FEM shell model in practical design as long as the localized deformation is moderate and not extremely large.

Regarding the vertical response of piers, the results obtained by the multiple spring model are

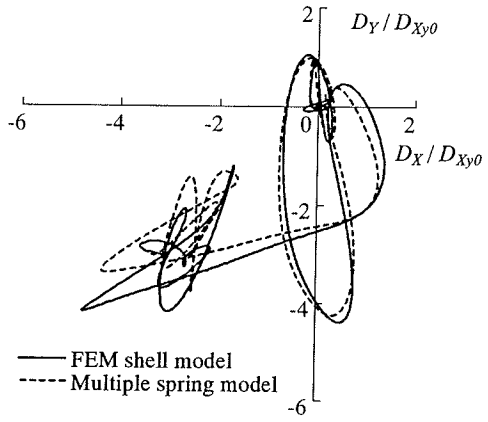

Fig.19 Trajectory of response sway displacement of pier 1 on *X-Y* plane under HKB wave

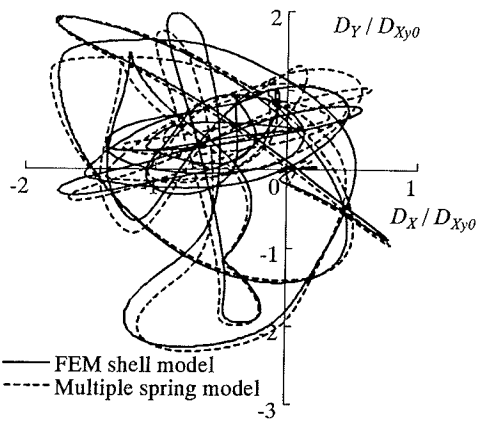

Fig.20 Trajectory of response sway displacement of pier 1 on *X-Y* plane under JMA wave

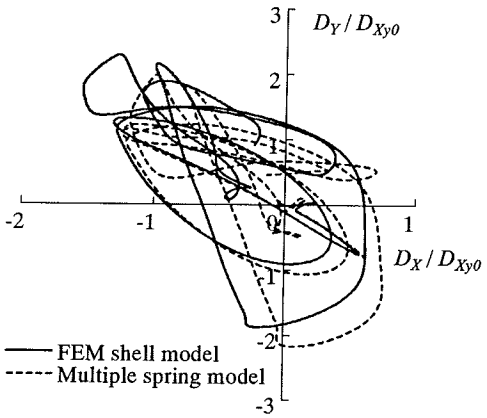

Fig.21 Trajectory of response sway displacement of pier 2 on *X-Y* plane under JMA wave

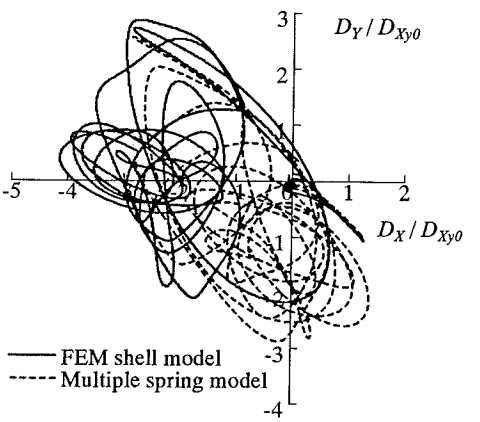

Fig.22 Trajectory of response sway displacement of pier 3 on *X-Y* plane under JMA wave

very different from those obtained by the FEM analysis as shown in **Fig.23**. One reason for this difference is that the constitutive relation for springs is calibrated not by the vertical displacement but by the horizontal displacement at the top of the pier. The other reason is that the magnitude of the vertical displacement is much smaller than that of the horizontal displacement. However, the vertical displacement predicted by the multiple spring model may have little effects practically because the vertical behavior is usually ignored in seismic design.

The residual displacement calculated by the multiple spring model also tends to be somewhat different from that by FEM analysis. This is because the residual displacement is very sensitive to the numerical errors and even small errors have a big influence on the final displacement.

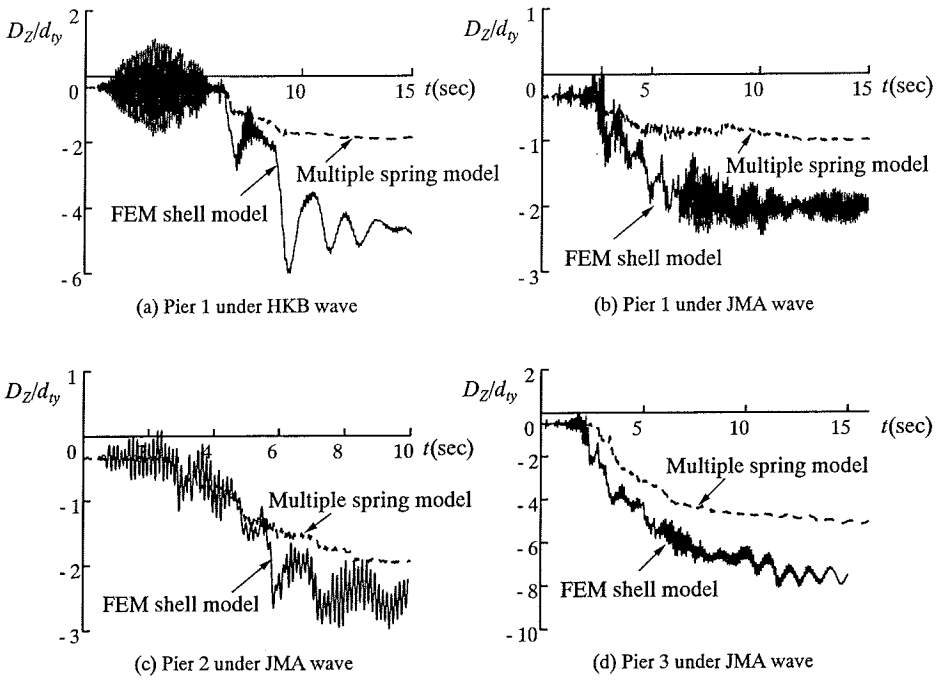

Fig.23 Time- vertical response displacements

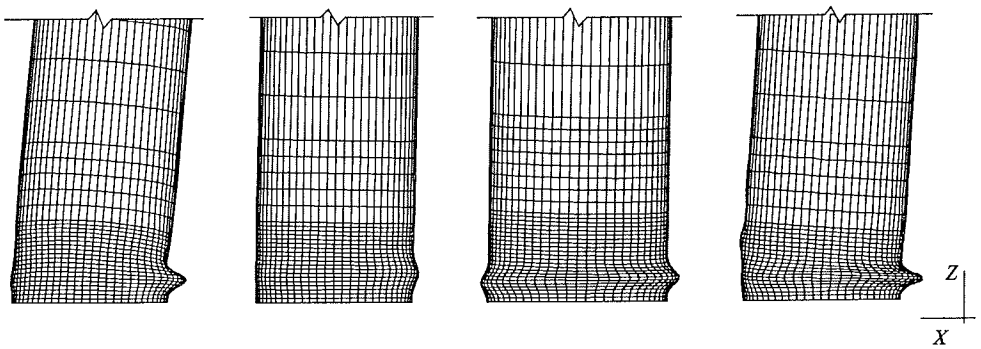

Fig.24 Deformation patterns at the bottom (displacement amplification factor=4)

5. CONCLUSIONS

In view of the application to the practical design, a multiple spring model is proposed to express the 3D-hysteretic behavior of moderately thin-walled piers. The model consists of a rigid pier and multiple nonlinear springs located at the pier base. These multiple springs can represent not only the interaction between the axial force and the biaxial

bending but also the local buckling effect. The constitutive relation for each spring is expressed by the multi-linear model and the parameters of this model are calibrated based on the in-plane hysteretic behavior of the 2-parameter model. In order to show the validity of the proposed model, 3-D earthquake response analyses are carried out by using both the multiple spring model and the FEM shell model. The results showed that the multiple spring model can be an acceptable alternative to the costly FEM shell analysis as long as the localized deformation is moderate and not extremely large. Furthermore, the computation time of the multiple spring model in the 3-D dynamic response analyses is drastically reduced to $1/5000 \sim 1/6000$ of the computation time of the FEM shell model.

NOTATION

A = cross-sectional area of the pier;
$d_{c_{ml}}$ = limiting value for d_{c_m};
$d_{t_{yl}}$, $d_{t_{yr}}$ = limiting values for d_{t_y};
ΔD_X, ΔD_Y, ΔD_Z = incremental displacement components at the top of the pier;
E = Young's modulus;
E_e, E_i = elastic energy and hysteretic energy in the i-th loading;
f_{c_y}, d_{c_y} = yield force and deformation of the compression side of skeleton curve of spring;
f_{c_m}, d_{c_m} = maximum force and deformation of the compression side of skeleton curve of spring;
f_{t_y}, d_{t_y} = yield force and deformation of the tension side of skeleton curve of spring;
Δf_i, Δd_i = incremental force and deformation of the i-th spring;
F_{Xm}, D_{Xm} = maximum force and displacement of the skeleton curve of the 2-parameter model;
F_{Xy}, D_{Xy} = yield horizontal force and horizontal displacement in X direction of the skeleton curve of the 2-parameter model;
F_{Xy0}, D_{Xy0} = yield horizontal force and horizontal displacement in X direction of the pier without vertical force obtained by the beam model;
ΔF_X, ΔF_Y, ΔF_Z = incremental force components at the top of the pier;
G = elastic shear modulus;
I = second moment of inertia of pier;
k_{ce}, k_{ch}, k_{cd} = stiffness in elastic range, hardening range and softening range respectively, at compression side of skeleton curve of spring;
k_{cdl}, k_{cdr} = limiting values for k_{cd};
k_{chl}, k_{chr} = limiting values for k_{ch};
k_i = tangent stiffness of the i-th spring;
k_{te}, k_{tp} = stiffness in elastic range and plastic range respectively, at tension side of skeleton curve of spring;
K_{Xe}, K_{Xp} = stiffness in elastic range and plastic range respectively, of the bi-linear model;
K_1, K_2, K_d = stiffness in elastic range, hardening range and softening range respectively, of the 2-parameter model;
L = length of the pier;
R = radius of thin-walled circular steel pier;
R_t = radius-to-thickness ratio parameter;
t = thickness of thin-walled circular steel pier;
α = empirical parameter of the 2-parameter model;
θ_i = angle specifies the location of the i-th spring;
κ = shear coefficient of the thin-walled circular steel pier;
λ = slenderness ration parameter;
μ = axial force ratio; and
σ_y = yield stress of steel.

REFERENCES

1) *Preliminary report on the great HANSHIN earthquake, January 17, 1995*, JSCE, 1995.
2) *Interim guideline and new technology for seismic design of steel highway bridges, committee on new technology for steel structures*, JSCE, (in Japanese), 1996.
3) Japan Road Association: *Specification for highway bridges – Part V seismic design*, Maruzen, Tokyo, 1996.
4) Liu, Q. Y., Usami, T. and Kasai, A.: Inelastic seismic design verification of thin-walled steel bridge piers, *NUCE Research Report No.9903*, Dept. of Civil Engineering, Nagoya University, 1999.
5) Liu, Q. Y., Kasai, A. and Usami, T.: Parameter identification of damage-based hysteretic model for pipe-section steel bridge piers, *Journal of Structural Engineering*, JSCE, 45A, pp. 1005-1016, 1999.
6) Watanabe, E., Sugiura, K. and Oyawa, W. O.: Effects of multi-directional displacement paths on the cyclic behavior of rectangular hollow steel columns, *Journal of Structural Mech. and Earthquake Engineering*, JSCE, No. 647/I-51, pp. 79-95, 2000.
7) Lai, S. S., Will, G. T. and Otani, S.: Model for inelastic biaxial bending of concrete members, *Journal of Structural Engineering*, ASCE, Vol.110, St11, pp. 2563-2584, 1984.
8) Wada, S. and Kinoshita, M.: Elastic plastic dynamic 3-dimensional response analysis by using a multiple shear spring model, *Symposium of the 9th Numerical Analysis Method in Structural Engineering*, pp. 317-322, (in

Japanese), 1985.
9) Ohi, K. and Takanashi, K.: Multi-spring joint model for inelastic behavior of steel members with local buckling, *Stability and Ductility of Steel Structures under Cyclic Loading*, edited by Y. Fukumoto and G. Lee, CRC Press, Florida, pp. 215-224, 1992.
10) HKS, Inc.: *ABAQUS/Standard User's Manual*, Version 5.8, Vol. I, II and III, 1998.
11) Goto, Y., Wang, Q. Y. and Obata, M.: FEM analysis for hysteretic behavior of thin-walled piers, *Journal of Structural Engineering*, ASCE, 124(11), pp. 1290-1301, 1998.
12) Gao, S. B., Usami, T. and Ge, H. B.: Ductility evaluation of steel bridge piers with pipe sections, *Journal of Engineering Mechanics*, ASCE, 124(3), pp. 260-267, 1998.
13) Suzuki, M. and Usami, T.: Fundamental study on the elastoplastic behavior of steel bridge piers, *NUCE Research Report No.9702*, Dept. of Civil Engineering, Nagoya University, (in Japanese), 1997.

(Received November 14, 2000)